

The Performance & Flow Visualization Studies of Three Dimensional (3-D) Wind Turbine Blade Models

Sutrisno¹, Prajitno¹, Purnomo¹ & B.W. Setyawan²

¹ Department of Mechanical and Industrial Engineering, Faculty of Engineering, Gadjah Mada University, Jl. Grafika 2, Yogyakarta 55281, Indonesia

² Department of Mechanical Engineering, Vocation Program, Gadjah Mada University, Yogyakarta 55281, Indonesia

Correspondence: Sutrisno, Department of Mechanical and Industrial Engineering, Faculty of Engineering, Gadjah Mada University, Jl. Grafika 2, Yogyakarta 55281, Indonesia. E-mail: mrsutrisnougm@gmail.com

Received: November 9, 2015

Accepted: November 25, 2015

Online Published: April 2, 2016

doi:10.5539/mas.v10n5p132

URL: <http://dx.doi.org/10.5539/mas.v10n5p132>

The research is financed by Department of Research, Technology, and Higher Education, Republic of Indonesia.

Abstract

The researches on the design of 3-D wind turbine blades have been received less attention so far even though 3-D blade products are widely sold. In the opposite, advanced researches in 3-D helicopter blade have been studied rigorously. Researches in wind turbine blade modeling are mostly assumed that blade span wise sections behaves as independent two dimensional (2-D) airfoils, implying that there is no exchange of momentum in the span wise direction. Further more flow visualization experiments are infrequently conducted.

The purpose of this study is to investigate the performance of 3-D wind turbine blade models with backward-forward swept and verify the flow patterns using flow visualization. In this research, the blade models are constructed based on the twist and chord distributions following Schmitz's formula. Forward and backward swept are added to the wind turbine blades. It is hoped that the additional swept would enhance or diminish outward flow disturbance or stall development propagation on the span wise blade surfaces to give better blade design.

The performance of the 3-D wind turbine system models are measured by a torque meter, employing Prony's braking system, and the 3-D flow patterns around the rotating blade models are investigated applying "tuft-visualization technique", to study the appearance of laminar, separated and boundary layer flow patterns surrounding the 3-dimensional blade system.

For low speed wind turbines, Dumitrescu and Cardos (2011) have identified that stall spreads from the root of the rotating blade. In this study, it is found that for blades with (i) forward swept tip and backward swept root, the initial stall at the blade bottom would be amplified by concurrent strengthening flow due to the backward swept root to create strong stall spreading outward, and therefore the blades gives lower performance. For blades with (ii) backward swept tip and forward swept root, the initial stall at the blade bottom would be weakened by opposite weakening flow due to the forward swept root, generate weak stall that tend to deteriorate. These blades have better performance.

Keywords: forward swept, tuft flow visualization, 3-D wind turbine blades, stall propagation

1. Introduction

The analyses of horizontal axis wind turbine (HAWT) aerodynamics assume that blade spanwise sections can be treated as independent airfoils operating in a 2-D, wind-tunnel-like flow condition. This assumption implies that there is no exchange of momentum in the spanwise direction. This has been proven to be a reasonable assumption for HAWT operating at medium to high tip speed ratios. Even helicopters, which operate in a highly 3-D flow state, can be analyzed using 2-D airfoil data (Butterfield, 1988).

So far the researchs in wind turbine system have been carried out on several aspects, such as the progress of the wind turbine blade design, the 3-D effect that influence the emergence of stall (Butterfield & Nelson, 1990),

(Butterfield, 1988), the optimization methods study (Chehouri et al., 2015), the theory about helical vortex structures leading to instabilities and vortex development in the blade root and tip (Sherry et al., 2013a, b), the helicopter propeller tip design review that should be alike with the 3-D wind turbine blade design philosophy (Brocklehurst & Barakos, 2013), as well as the progress of materials and the process of the blade manufacture of the wind turbines (Suzan and Tusavul, 2014).

Some scientific publications in wind turbine researches progress have been reported. Chehouri et al. (2015) have elucidated the review of performance optimization techniques applied to wind turbines. A method combining the blade element momentum (BEM) theory and a vortex theory assuming small perturbation have been proposed. This model has been used in many tools for the calculation of the aerodynamic loadings because of its accuracy, simplicity and ease of intuitive understanding. Finally, modeling and measurements of wind turbine wakes in wind tunnels have been conducted using hot wire anemometry or particle image velocimetry. Recently, in computational fluid dynamics (CFD) modeling, the free vortex wake method has been applied to wind turbines. It is more demanding than the BEM in terms of computational time. The flow field around the rotor, both upstream and downstream can be modeled by on viscous methods as long as the vorticity is accounted for. In wide range of cases, blade design with 2-D BEM needs some improvement and full 3-D theory is truly in demand.

Blade design and performance testing of a small wind turbine rotor utilizing BEM theory for low wind speed applications, have been reported by Ronit et al. (2013). The use of specially designed low Reynold number (Re) airfoils permits start up at lower wind speeds, increasing the startup torque and thus improving the overall performance of the turbine. Another blade design and performance testing of a small wind turbine rotor for low wind speed applications have been conducted by Singh and Ahmed (2013).

Design of 10 kW HAWT blade and aerodynamic investigation using numerical simulation have been performed by Bai et al. (2013). Improved BEM theory including Viterna-Corrigan stall model, tip-loss factor and stall delay model has been developed for predicting the performance of the designed turbine blade. There is a good comparison of torque and thrust in each section between the improved BEM theory and numerical simulation. Design and experimentation of a 1 MW HAWT have been described by Velázquez et al. (2014). It could be shown that the experimental data can improve BEM theory to achieve better results by adjusting factors. For design purposes of large scale wind turbines, combined theory for the design of the blades is not sufficient to ensure optimum performance for power generation. To achieve an efficient design, other design techniques applying the BEM simple qualities should be used. Combining BEM and any optimization algorithm is more advisable to develop a more sophisticated design. Comparison of BEM and CFD results for Mexico rotor aerodynamics has been reported by Plaza et al. (2015). These reports are very close to 2-D assumption. These reports are mostly investigation of 2-D blade cases. Would one still confident that BEM theory also applicable to 3-D wind turbine blades, where the blade has swept features whether in the blade tip or root.

Combine flow visualization experiments such as aerodynamic pressure and flow-visualization measurement from a rotating wind turbine blade applying tuft method have been reported by Butterfield (1988) and Butterfield and Nelsen (1990). Hirahara et al.(2005), has reported testing basic performance of a very small wind turbine designed for multi-purposes. By the flow visualization and PIV measurement around the wind turbine, the approaching flow velocity and the accelerated flow field passing the blade tip have been obtained. Only few flow visualization studies in wind turbine blades have been reported.

1.1 The Early Research in Wind Turbine Blades

At early research development of the rotor theory, the simple momentum theories were not sufficient to design propeller blade, whereas it was the most important rotor configuration of the time. Therefore, specific design method was developed, on the basis of the dividing a blade into a number of spanwise sections and using vortex theory to determine the induced velocities. This method for infinitely many blades was called the BEM theory. Tip correction, or tip loss factor, was introduced by Glauert for finite number of blades. The development continued with a derivation of the Kutta-Joukowski theorem for a cascade of blade elements and applied to lifting line theory of rotors with finite number of blades to arrive to the final results (Okulov et al., 2006).

The result obtained by the BEM method was reasonably accurate in the proximity of the design point, but in stalled condition the BEM was under predict the force acting on the blades. The major disadvantage of these methods according to Glauert was that the airflow reduced to axial and circumferential flow components. NASA report showed that approaching the rotational axis, the Coriolis force in the cross flow direction became more important. On the other hand the contribution of centrifugal pumping effect increased particularly in the region of the separated flow. Dumitrescu and Cardoso (2009) studied the boundary layer behavior very close to the

rotation center ($r/c < 1$). It was identified that the stall delay depended strongly on the leading edge separation bubbles formed on inboard blade segment due to a suction effect at the root area of the blade (Dumitrescu & Cardoso, 2011).

Several recent studies on wind turbine blade flow dynamics were focused on CFD modeling on stall delay, the role of centrifugal force and Coriolis force due to rotation postponed separation point (Hu et al., 2006). With the help of the surface limiting streamlines, low and high speed of the wind generated blade root and tip flows (Yu et al., 2011).

1.2 The Growth of Wind Turbine Blade Stall

At low wind speed conditions, Dumitrescu and Cardoso (2011) concluded that the visualization of the flow was well-behaved and attached over much of the rotor. They showed the separated area and radial flow on the suction side of a commercial blade, as shown in Figure 1. The secondary flow was strongest at approximately 0.17 and reached up to 0.31 the rotor radius.

At low wind speed, the main rotational effect is due to the Coriolis force which delays the occurrence of separation to a point further downstream towards the trailing edge, and by this the suction pressures move towards higher levels as r/c decreases.

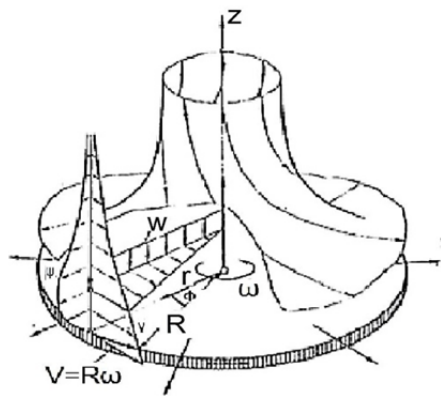


Figure 1. Pumping-work mode of a wind turbine at low wind speeds ($X > 3.0$). The concept of flow close to a rotating disk in a fluid at rest

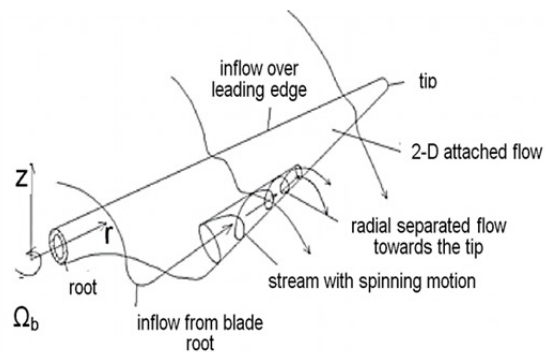


Figure 2. For low speed wind turbines, Dumitrescu and Cardoso (2011) have identified that stall spreads from the root of the rotating blade. The sketch of the model of the separation flow

The pressure field created by the presence of the turbine is related to the incoming flow field around the blade, taken as being composed of the free wind velocity and the so-called induction velocity due to the rotor and its wake. Thus, the incoming field results from a weak interaction between two different flows: one axial and the other rotational. In such a weak interaction flow, the basic assumptions made are: (i) the radial independence principle is applied to flow effects, i.e. induction velocities used at a certain radial station depend only on the local aerodynamic forces at that same station, (ii) the mathematical description of the air flow over the blades is based on the 2-D flow potential independent of the span, and on corrections for viscosity and 3-D rotational effects.

These assumptions suitable to BEM methods reduce the complexity of the problem by an order of magnitude yielding reliable results for the local forces and the overall torque in the proximity of the design point, at high tip speed ratios. In order to estimate the 3-D rotational effects, usually neglected in the traditional BEM model, the flow around a hypothetical blade with prestall/stall incidence and chord constant along the whole span is considered in the sequel.

1.3 Stall Propagating Scheme

In order to simulate the 3-D stall delay effects, the effect of rotation on the boundary layer of a wind turbine blade, Du and Selig (2000), developed model for adjusting the 2-D airfoil data. The 3-D integral laminar boundary layer equations for a rotating reference frame were analyzed. In this model, the 3-D lift (C_l) and drag (C_d) coefficients could be expressed as the 2-D lift and drag coefficients plus increments in lift and drag coefficients, $C_l(3D) = C_l(2D) + \Delta C_l$ and $C_d(3D) = C_d(2D) + \Delta C_d$.

Several researches simulating the 3-D stall delay effects works have been reported. For low speed wind turbines, Dumitrescu and Cardos (2011) have identified that stall spreads from the root of the rotating blade, Fig. 2. A study of the energetic turbulence structures during stall delay has been investigated by Wua et al. (2015). A study on stall-delay for horizontal axis wind turbine, has been reported by Hu et al. (2006). The computation results show that rotation affects the pressure distribution on the surface of the foil, which can give rise to 3-D stall-delay in stalled condition. An investigation of the stall mechanisms on stall-delay has been conducted by Sicot et al. (2008), proposing a method to determine the position of the separation point on the rotating blade, based on the chordwise pressure gradient in the separated area. The results show an influence of the free stream turbulence level on the separation point position. An experimental study of stall delay on the blade of a HAWT using tomographic particle image velocimetry has been reported by Lee and Wu (2013).

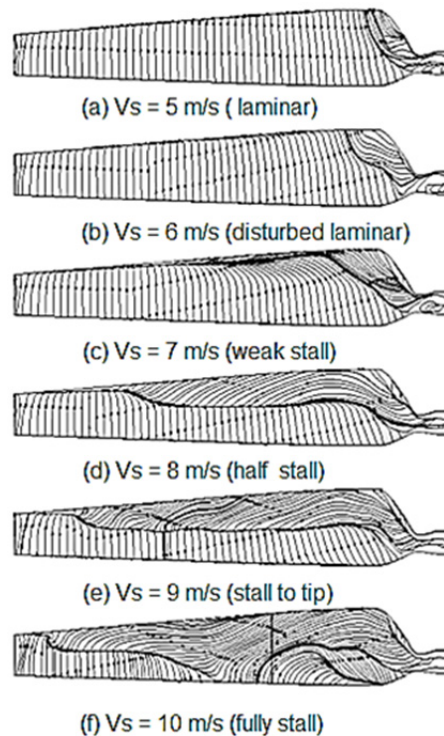


Figure 3. Limiting streamlines distribution on the blade suction surface (Yu et al., 2011 with modification)

Consecutive modeling of inboard stall delay due to rotation has been considered by Dumitrescu and Cardoso (2002, 2009) and Dumitrescu et al. (2007). These reports give a conceptualization of the complex 3-D flow field on a rotor blade, where stall begins and how it progresses, driven by the needs to formulate a reasonably simple model that complements the 2-D airfoil characteristics used to predict rotor performance.

Yu et al. (2011) have carried out CFD investigation on the flow characteristics and the stall delay phenomenon of wind turbine rotor due to blade rotation, at different wind speeds from 5 m/s to 10 m/s. Fig. 3 presents the boundary flow topology of blade suction surface at different wind speeds with the help of surface limiting streamlines which is often applied to depict surface flow status.

Below 7 m/s, the limiting streamlines are oriented parallel to the chord wise direction, indicating that the flow is fully attached and resembles a 2-D flow. Only in the region very close to the root, shows the flow a weak 3-D. With the wind speed increased to 7 m/s, the weak stall, flow separation initiates near the trailing edge, and the radial flow takes over a larger area of the blade inboard portion, however the chord wise 2-D flow is still predominant. The separation line moves forward towards leading edge, toward stall-to-tip state, and span wise flow spreads to the outboard of the blade, the half stall area, as the wind speed enhances further to 9 m/s. When the incoming wind speed rises up to 10 m/s, at fully stall state, flow separates at the leading edge in the inboard half part. Chord wise flow shrinks to a very limited area of the front outboard part. Span wise flow now becomes

dominant and extends to most part of the suction surface.

The complex 3-D flow field on a rotor blade, where stall begins and how it progresses, have been formulated to give a reasonably simple model that complements the 2-D airfoil characteristics used to predict rotor performance. It is unfortunate that these complex 3-D flow field formulations on a rotor blade, have not been extended to more general cases, 3-D blade modeling, such as the effect of crooked or bent blades, the effect of forward and backward sweeps of rotating wind turbine blades.

The purpose of this study is to investigate the performance of 3-D wind turbine blade models and verify the flow patterns using flow visualization. In this paper, the effect of forward and backward sweeps of rotating wind turbine blades became the main focus of the current investigation. The wind turbine systems, with rotating 3-D blade models, were investigated in 30cm x 30cm and 50cm x 50cm wind tunnels. It was known in wing aerodynamics that the back-swept effect would enhance outward span-wise spread of the flow disturbance on the wing surface, while the forward-swept effect would diminish the outward flow propagation. It is expected that this investigation would lead to better performance of wind turbine blades especially the 3-D blade design and can be applied to better design of large and small wind turbine systems.

The outcomes of this investigation would open research opportunity for i) 3-D blade tips of large wind turbines similar to advanced study for the blade tips of helicopters, and ii) 3-D small wind turbine blades in general for performance enhancements.

2. Experimental Apparatus and Procedures

The main objective of this investigation was to analyze the wind turbine blade models characteristics in the wind tunnels. The experiments would consist of blade models performance measurements and thorough full investigation of the flow visualization to conform the data against several identified stall types to determine their flow characteristics, to find better qualifications for the turbine blade models.

The performance of the 3-D wind turbine blade models were measured in the wind tunnel, using a torque meter, Fig. 4, a prony-type brake method. In order to confirm the performance of the 3-D models, the “tuft” flow visualization technique was applied. The Nikon J3 camera was used to record the blade motion at 1200 frames/second.

Implementing the correlation between C_p versus the tip speed ratio of the turbine, against the results of flow visualization technique, one could study the appearance of the laminar patterns, the patterns of weak stall, half and fully stalled, and re-attached boundary layer flows surrounding the 3-D blade system.

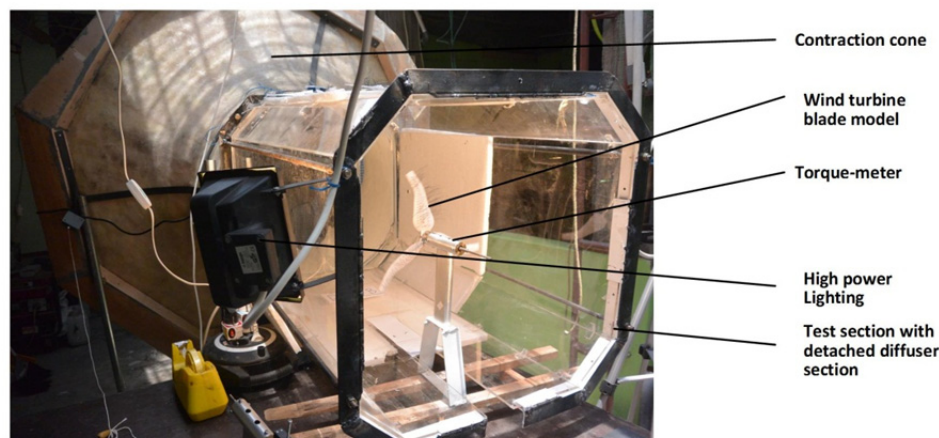


Figure 4. The torque meter installed in the wind tunnel, to measure the performance of the blades

2.1 Experiment Preparation

The experimental program began with wind turbine blade design following the blade chord and twist distributions of Schmidtz blade model. Two 3-D bent blade configurations, as shown in Fig.5, were investigated. The blade C, the blade bent closed to the root and the blade D, the blade bent close to the tip, each was in combination with backward-forward sweeps at the tip and the root of the blades. These combinations were expected to contribute better 3-D favourable rotational force of the rotor system.

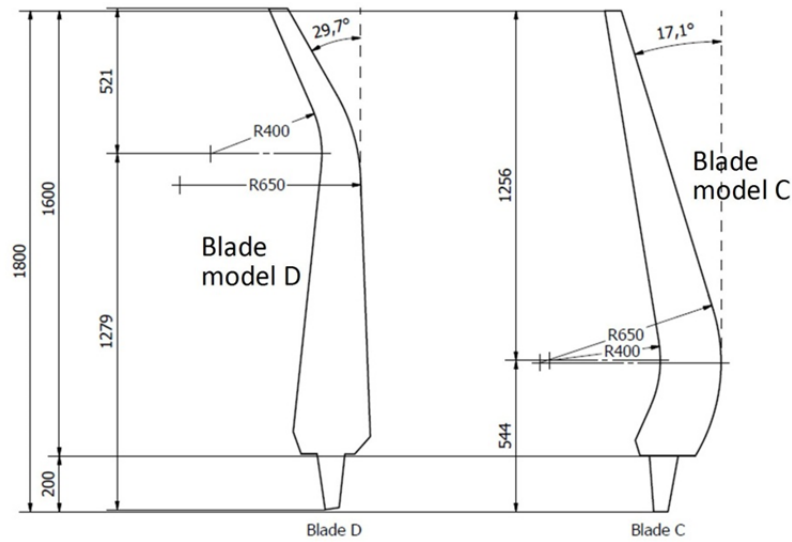


Figure 5. Size outline of the blade model C (right) and D (left), with backward-forward sweeps at the tip and the root of the blades

Fig. 5 shows the size outline of the wind turbine blade models C and D. Blade C_{bwd} is blade C with forward root and backward tip, C_{fwd} is blade C with forward tip and backward root, D_{bwd} is blade D with forward root and backward tip, while D_{fwd} is blade D with forward tip and backward root. The wind turbine blade model, the blade C and D, have 28 cm diameter, with hub diameter = 5 cm. The profile of airfoil section of the models is NACA 4412. The Fig. 6 is the Schmitz' type chord distribution of the blade model, and the linearization or size reduction of the blade chord near the root (Velázquez, 2014).

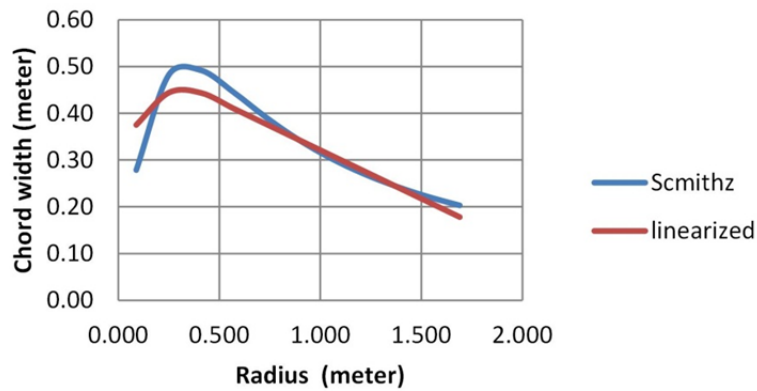


Figure 6. Chord distribution & the size reduction of the chord near the root

2.2 The Model Performance Measurement in Wind Tunnels

The rotation per minute, RPM, ω , or the frequency of the rotating wind turbine models was measured by digital tachometer. The torque, in Nm, $\tau = (9.81 \times 10^{-6}) l \times f$, of the wind rotor models was measured using a torque meter, the prony-type brake system. The wind speed, v_1 in m/s, was measured by Pitot tube and wall static pressure system. Here, l in millimeter is the length of torque arm and f is the load measured by weight scale, in gram.

From the RPM and wind speed, v_1 , one could find the tip speed ratio of the turbine, X , applying the outer blade rotational speed, ωR , divided by v_1 , where R is the outer radius of the blade. The output power of wind turbine, P_T , would be calculated by multiplying the torque with the RPM, and from the turbine power, one could calculate the coefficient of performance, C_p as,

$$P_T = \frac{9.81 \times 2\pi}{60} \times 10^{-6} \times l \times f \times \text{RPM}; \quad \tau = (9.81 \times 10^{-6}) \times l \times f \quad (1)$$

$$C_p = \frac{P_T}{P_w} = \frac{10^6 \times P_T}{\frac{1}{2} \rho v_1^3 \cdot \pi R^2}, \quad \text{and} \quad X = \frac{2\pi}{60} \times 10^{-3} \times \text{RPM} \times R / v_1 \quad (2)$$

Where P_w is the wind power (W), v_1 is the free stream velocity (m/s), ρ is the air density (kg/m^3), and R is the rotor radius (mm).

Wind turbine power and coefficient of power C_p could be evaluated from equations (1) and (2) respectively. The atmospheric pressure was taken as standard: 101.3 kPa. An average ambient temperature of 25°C was recorded. According to the gas equation, the air density and temperature are related. One could find the air density to be 1.184 kg/m^3 . In the present experimental study, the air pressure and temperature were kept constant. Those were measured in a perfect laboratory conditions, therefore, it is noticed that the air density was not changed.

2.3 Flow Visualization of 3-D Wind Turbine Blade Model Using Tuft Method

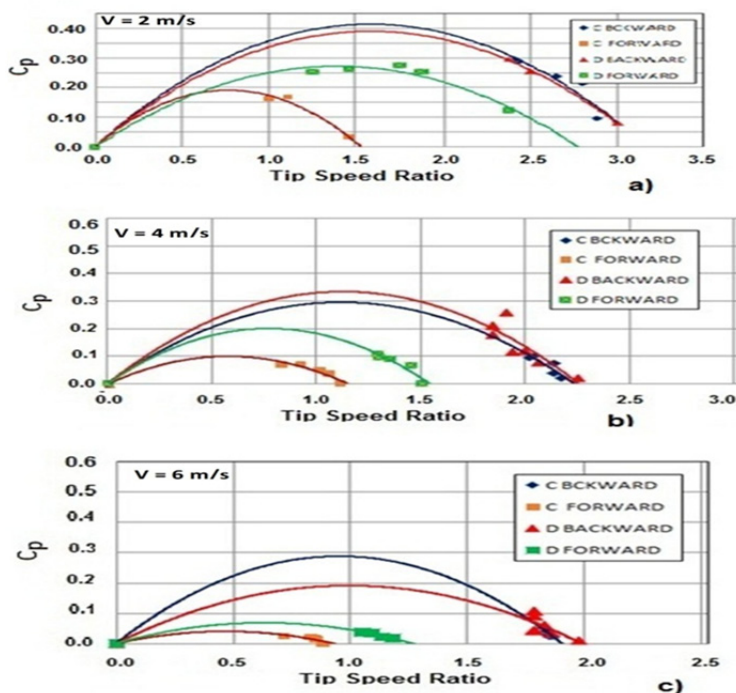
In order to understand the effectiveness of wind energy conversion into the rotation energy of the generator, a tuft flow visualization method was carried out to study flow surrounding the forward and backward C and D wind turbine blade models. The test examined the pattern of the flow caused by the blade disturbance.

The blade model was drilled 2 to 4 rows span wise, with 4 mm distance in between. Regular sewing yarn was used as tuft material, split into three parts and inserted into the holes to create several rows of tuft arrange in lines. The length of the tuft varies from 2 cm to 6 cm whenever necessary. As air flows around the blades, the rows of tuft would show the flow patterns surrounding the blade models.

3. Results

3.1 Performance Measurement of 3-D Wind Turbine Blade Models

From the torque measurements of the wind turbine blade models, one could determine the blades model performances that might be presented as in Fig. 7 a, b, c and d showing coefficient of performance, C_p versus tip speed ratio, X , for blade models at wind speed a) 2 m/s, b) 4 m/s, c) 6 m/s and d) 8 m/s at Reynolds number, $Re = 1.663 \times 10^3$ to 6.665×10^3 .



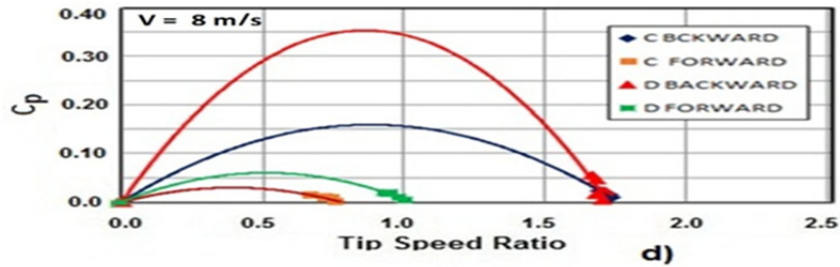


Figure 7. The wind turbine blade models performance, coefficient of performance C_p versus tip speed ratio, X , between the four blades, C_{bwd} , C_{fwd} , D_{bwd} and D_{fwd} , for wind speed. a) 2 m/s, b) 4 m/s, c) 6 m/s and d) 8 m/s

Fig. 7 a, b, c and d show the performance coefficient comparison between the four blades, C_{bwd} , C_{fwd} , D_{bwd} and D_{fwd} at wind speed a) 2 m/s, b) 4 m/s, c) 6 m/s and d) 8 m/s. In Fig. 7 the dimensionless coefficient of power, C_p , is plotted against the tip speed ratio, X . From this figure, it is found that backward swept blade models C_{bwd} and D_{bwd} gives better performance than forward swept blade models C_{fwd} and D_{fwd} at all wind speeds considered.

Eventhough only limited qualitative amount of data are needed for verification in this experiment, large amount of quantitative data has been measured. Therefore this work has a significant effect to establish a new data base for upcoming investigation and future design of wind turbine blade.

3.2 Flow Visualization to Verify the Turbine Blade Models Performance

In order to investigate the important role of the propagating stall of the forward and backward swept blade models, the stall that was originated from the blade root trailing edge, could be revealed using tuft flow visualization technique. The flow patterns surrounding the forward and backward C and D blade models could be studied to see the passage of the stall propagation, the direction of the flow by analyzing the tuft bending direction. Several types of stall patterns were identified during investigation, in conjunction with the limiting streamlines distribution on the blade suction surface, shown in Fig. 2. The four stall patterns were shown in Fig. 8.

Fig 8 a) shows laminar type flow pattern. The tuft pattern demonstrates smooth, laminar flow on the root surface of the blade, the tuft do not show significant moves. Fig. 8 b) shows the type of flow with weak stall, where the wave of the tuft indicates slow, gentle movement on the blade root surface.

In Fig. 8 c) the tuft wave shows the half stall type flow, shown by tuft upward direction close to trailing edge, with 2 or 3 vertical columns of tuft pointing upward, aligns almost up to the blade tip. While Fig. 8 d) shows the stall-to-tip type flow until fully stall, where the wave of almost all vertical columns close to the trailing edge of tuft aligns upward with wavy movements.

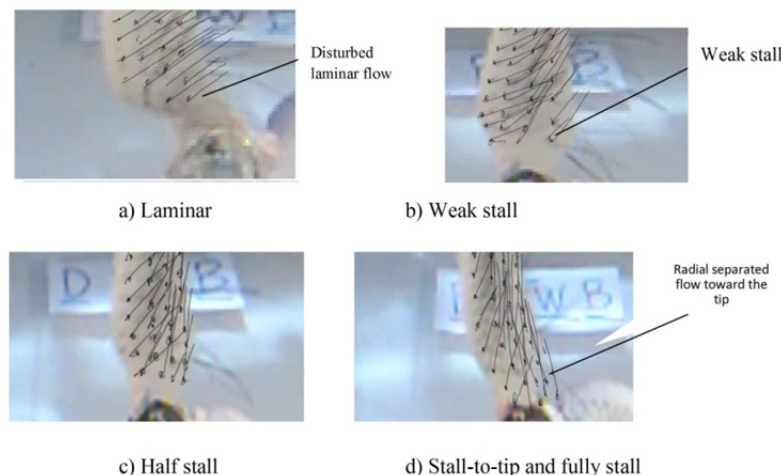


Figure 8. Several types of stall were identified a) laminar type flow, b) flow with weak stall, c) flow with half stall and d) flow with stall to the tip or fully stall flow, in accordance with Fig. 2 a, b, c, d, e and f of Yu et al. (2011)

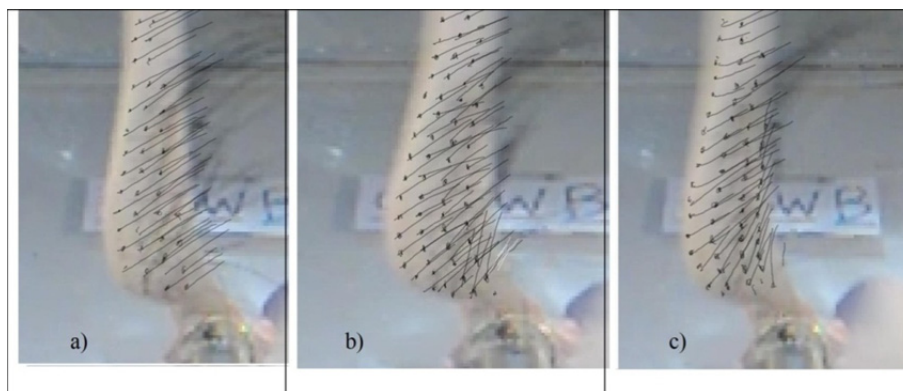


Figure 9. Sketches of the tuft pattern of the blade C, with backward swept tip, rotating in wind tunnel a) at wind velocity = 2.5 m/s, RPM = 870, b) at wind velocity = 3.0 m/s, RPM = 1070, and c) at wind velocity = 3.5 m/s, RPM = 1450

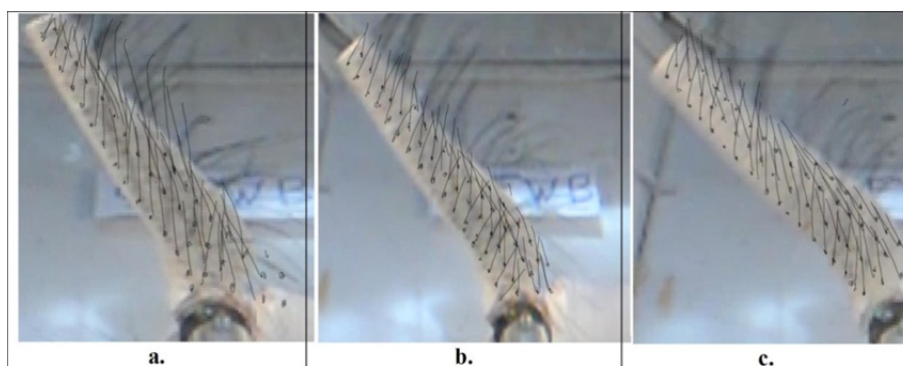


Figure 10. Sketches of the tuft pattern of the blade C, with forward swept tip, rotating in wind tunnel a) at wind velocity = 2.5 m/s, RPM = 650, b) at wind velocity = 3.0 m/s, RPM = 800, and c) at wind velocity = 3.5 m/s, RPM = 1140

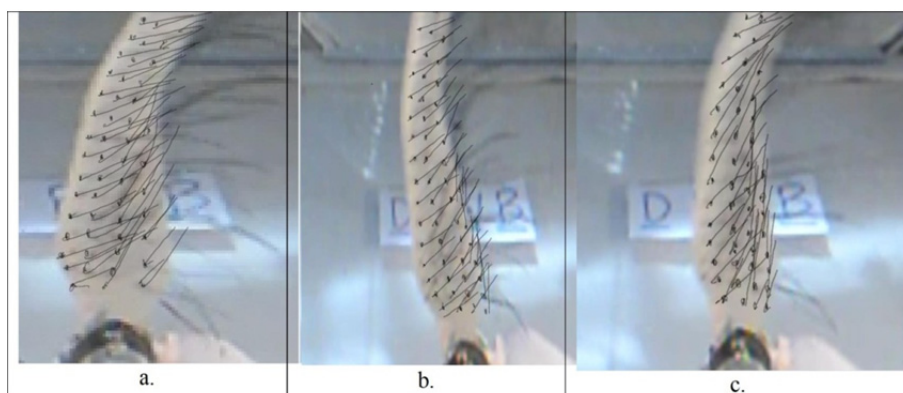


Figure 11. Sketches of the tuft pattern of the blade D, with backward swept tip, rotating in wind tunnel a) at wind velocity = 2.5 m/s, RPM = 640, b) at wind velocity = 3.0 m/s, RPM = 830, and c) at wind velocity = 3.5 m/s, RPM = 1090

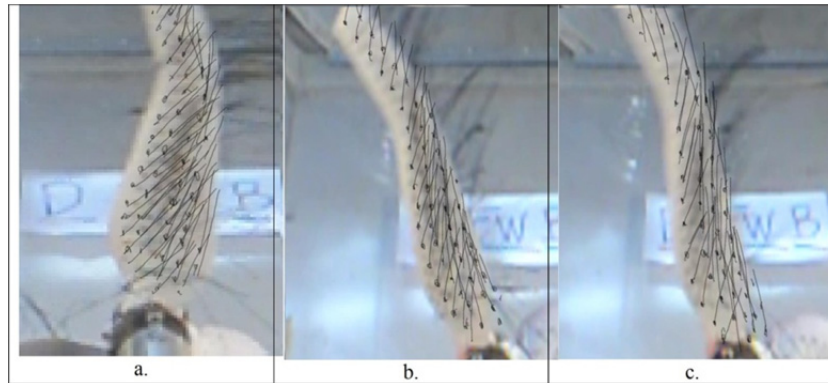


Figure 12. Sketches of the tuft pattern of the blade D, with forward swept tip, rotating in wind tunnel a) at wind velocity = 2.5 m/s, RPM = 600, b) at wind velocity = 3.0 m/s, RPM = 830, and c) at wind velocity = 3.5 m/s, RPM = 1100.

From the result of flow visualization studies, one could recognize that Fig 9 a) to d) demonstrate the sketches of the tuft pattern of the blade C_{bwd} rotating in the wind tunnel at wind velocity = 2.5 m/s, RPM = 870, b) at wind velocity = 3.0 m/s, RPM = 1070, and c) at wind velocity = 3.5 m/s, RPM = 1450. They show the flow surrounding the blade C_{bwd} in laminar to weak stall conditions. Fig 10 a) to d) illustrate also the sketches of the tuft pattern of the blade C_{fwd} rotating in the wind tunnel at wind velocity = 2.5 m/s, RPM = 650, b) at wind velocity = 3.0 m/s, RPM = 800, and c) at wind velocity = 3.5 m/s, RPM = 1140. They explain that the flow surrounding the blade C_{fwd} in half-stall to stall to tip and full stall conditions.

One could identify also that Fig. 11a) to d) clarify that the flow surrounding the blade D_{bwd} in laminar to weak stall conditions while Fig. 11a) to d) explain that the flow surrounding the blade D_{fwd} in half-stall to stall to tip and fully stall conditions.

4. Discussion

From Fig. 9 to 12, one could learn the comparison between the four blades, C_{bwd} , C_{fwd} , D_{bwd} and D_{fwd} , that is the role of blade root and tip forward swept and root and tip backward swept on the stall propagation originated from the root trailing edge of the 3-D wind turbine blade models.

In combination with the wind turbine blade models performance shown in Fig. 7 a) to d), one can conclude that the blade C_{bwd} and blade D_{bwd} have superior performance, where both have root forward swept and tip backward swept. The same conclusion could be drawn from the flow visualization comparison Fig 8 to 12a) to c).

And it is shown also in the flow visualization results, Fig. 9, that the C_{bwd} , with root forward swept, would tend to diminish the outward weak stall flow propagation, and further more since at the bent the flow is almost laminar to weak stall, the blade root backward swept would only convey very weak disturbance. The same process occurs on blade D_{bwd} , shown in Fig. 11, since the blade is also with root forward swept and tip backward swept. The major differences are, the bent of the blade C is close to the root, the angle of root forward swept is much steeper here, therefore the weak stall disturbance would be even weaker compared with the disturbance on blade D_{bwd} .

The opposite happens at blade C_{fwd} and D_{fwd} . The blade C_{fwd} is with tip forward swept and root backward swept. The root backward swept of the blade would tend to enhance the outward stall flow propagation, and further more since at the bent the flow is almost half stall, the blade root forward swept would still propagate significant wavy disturbances.

The same process occurs also on blade D_{fwd} , shown in Fig. 12, the blade is also with tip forward swept and root backward swept. The main differences are, the bent of the blade D is close to the tip, the angle of root backward swept is much steeper therefore the half stall disturbance would be even stronger with significant amplification toward wobble turbulence.

It is believed that the wavy disturbance is a direct result of the collision between the incoming flow against the outward disturbance propagation following blade tip forward swept. It would cause instability-like movement of the tuft in the flow visualization.

Table 1. Flow visualization mapping of flow surrounding 3-D wind turbine blade models

Figure no.	blade name	wind vel. m/s	blade tip swept	blade RPM	Reynolds number: $Re \cdot 10^{-3}$	Stall propagation pattern due to blade bent	degree of turbulence	Stall type / flow characteristic
						Close to Tip		
Fig 9a	C	2.5	backward	870	2.078	 WSDL	weak	Disturbed laminar
Fig 10a	C	2.5	forward	650	2.078	 SSTWF	strong	Stall-to-tip/ Wavy flow
Fig 9b	C	3.0	backward	1070	2.494	 WSDL	weak	Disturbed laminar
Fig 10b	C	3.0	forward	800	2.494	 SSTWF	strong	Stall-to-tip/ Wavy flow
Fig 9c	C	3.5	backward	1450	2.910	 WSDL	weak	Weak stall/Stall delay
Fig 10c	C	3.5	forward	1140	2.910	 SSTWF	strong	Stall-to-tip/ Wavy flow
						Close to Root		
Fig 11a	D	2.5	backward	640	2.078	 WSMTL	weak	Weak stall/Stall delay
Fig 12a	D	2.5	forward	600	2.078	 SSTWF	strong	Stall-to-tip/ Wavy flow
Fig 11b	D	3.0	backward	830	2.494	 WSMTL	weak	Half stall/Stall delay
Fig 12b	D	3.0	forward	830	2.494	 SSTWF	strong	Stall-to-tip/ Wavy flow
Fig 11c	D	3.5	backward	1090	2.910	 WSMTL	weak	Half stall/Stall delay
Fig 12c	D	3.5	forward	1100	2.910	 SSTWF	strong	Full-stall/ Wavy flow

The result of flow visualization shown from Fig. 7 to 12 d) could be summarized and presented on Table 1 showing the blade name, type of blade tip swept, blade RPM, Reynolds number, stall propagation patterns due to the blade bent, degree of turbulences and stall types or flow characteristics. The abbreviations appear on the table have the following meanings, WSDL is weak stall with disturbed laminar pattern, WSMTL is weak stall disturbance with moderate transitional laminar, and SSTWF is strong stall to tip with wavy flow.

The research outcome opens investigation opportunity for i) 3-D blade tips of large wind turbines similar to advanced study for blade tips of helicopters, and ii) 3-D small wind turbines in generals for performance enhancements.

5. Conclusion

It can be concluded that, for low speed wind turbines, stall spreads from the root of the blade (Dumitrescu and Cardos, 2011). At least for the range considered in this study, for blades with (i) forward swept tip or backward swept root, D_{fwd} and C_{fwd} , the initial stall at blade bottom would be amplified by the backward swept to create strong stall spreads outward, and after the bent, the forward swept at blade tip would create wavy, unstable flow, and therefore the blade has low performance.

When the bent close to the root, such as a) the forward swept blade C_{fwd} , strong stall created by root backward, after the bent the strong stall would still spread to form stall-to tip. Similar happens when the bent close to the tip, such as b) the forward swept blade D_{fwd} , the difference is for the case blade D_{fwd} after the bent the stall would be somewhat weaker.

For blades with (ii) tip backward swept or root forward swept, D_{bwd} and C_{bwd} , the initial stall at blade bottom would be weakened by the forward swept, generate weak stall, and tend to deteriorate. The stall would be hard to spread to reach the bent. It was thought to cause inboard stall delay. As the speed grew faster the growing stall getting stronger and after the bent, the blade tip backward swept would amplify the disturbed flow. In general these blades have better performance.

Acknowledgments

This work has been carried out with a support of the Department of Higher Education, Republic of Indonesia. The authors would like to express sincere gratitude to Dr. Deendarlianto for time spent in serious discussion, helpful suggestion and useful conceptual contribution. We would like to thank also our students Abshar, Widia, Fadel, Fadhil, Dhanu, Surya, Ardi, Hasan, Andriyanto my laboratory staffs, Waji and Min, their helps in construction work and conducting data management are gratefully acknowledged.

References

- Bai, C. J., Hsiao, F. B., Li, M. H., Huang, G. Y., & Chen, Y. J. (2013). Design of 10 kW Horizontal-Axis Wind Turbine (HAWT) Blade and Aerodynamic Investigation Using Numerical Simulation. *Procedia Engineering*, 67, 279-287. <http://dx.doi.org/10.1016/j.proeng.2013.12.027>
- Brocklehurst, A. G., & Barakos, N. (2013). A review of helicopter rotor blade tip shapes. *Progress in Aerospace Sciences*, 56, 35–74. <http://dx.doi.org/10.1016/j.paerosci.2012.06.003n>
- Butterfield, C. P., & Nelsen, E. N. (1990). Aerodynamic Testing of a Rotating Wind Turbine Blade, SERI/TP-257-3490 UC Category: 261 DE90000312
- Butterfield, C. P. (1988). Aerodynamic Pressure and Flow-Visualization Measurement from a Rotating Wind Turbine Blade, SERI/TP-217-3433 UC Category: 261 DE89000854
- Chehouri, A., Younes, R., Ilinca, A., & Perron, J. (2015). Review of performance optimization techniques applied to wind turbines. *Applied Energy*, 142, 361–388. <http://dx.doi.org/10.1016/j.apenergy.2014.12.043>
- Du, Z., & Selig, M. S. (2000). The effect of rotation on the boundary layer of a wind turbine blade. *Renewable Energy*, 20, 167-181, PII: S0 96 0 -1 48 1 (99) 00 1 09 -3
- Dumitrescu, H., & Cardoso, V. (2011). Inboard Stall Delay Due to Rotation, Fundamental and Advanced Topics in Wind Power, Dr. Rupp Carriveau (Ed.), ISBN: 978-953-307-508-2
- Dumitrescu, H., & Cardoso, V. (2009). Inboard boundary layer state on wind turbine blades. *ZAMM*, 89(3), 163-173.
- Dumitrescu H., & Cardoso V. (2002). Delayed Stall Modelling of the Rotating Blades. *Proceedings of the Romanian Academy, Series A*, 12(2), 100–108.
- Dumitrescu, H., Cardoso, V., & Dumitrache, A. (2007). Modeling of inboard stall delay due to rotation, The Science of Making Torque from Wind. *Journal of Physics: Conference Series*, 75, IOP Publication. <http://dx.doi.org/10.1088/1742-6569/1/012022>.
- Hirahara, H., Hossain, M. Z., Kawahashi, M., & Nonomura, Y. (2005). Testing basic performance of a very small wind turbine designed for multi-purposes, *Renewable Energy* 30, 1279–1297. <http://dx.doi.org/10.1016/j.renene.2004.10.009>
- Hu, D., Hua, O., & Du, Z. (2006). A study on stall-delay for horizontal axis wind turbine. *Renewable Energy*, 31, 821–836. <http://dx.doi.org/10.1016/j.renene.2005.05.002>
- Lee, H. M., & Wu, Y. (2013). An experimental study of stall delay on the blade of a horizontal-axis wind turbine using tomographic particle image velocimetry. *Journal of Wind Engineering and Industrial Aerodynamics*, 123, 56–68. <http://dx.doi.org/10.1016/j.jweia.2013.10.005>
- Okulov, V. L., Sørensen, J. N., & Wood, D. H. (2014). The rotor theories by Professor Joukowsky: Vortex theories. *Progress in Aerospace Sciences*, 1–28. <http://dx.doi.org/10.1016/j.paerosci.2014.10.002>
- Plaza, B., Bardera, R., & Visiedo, S. (2015). Comparison of BEM and CFD results for MEXICO rotor aerodynamics. *Journal of Wind Engineering and Industrial Aerodynamics*, 145, 115–122. <http://dx.doi.org/>

10.1016/j.jweia.2015.05.005

- Sherry, M., Nemes, A., Jacono, D. L., Blackburn, H. M., & Sheridan, J. (2013a). The interaction of helical tip and root vortices in a wind turbine wake. *Physics of Fluids*, 25, 117102. <http://dx.doi.org/10.1063/1.4824734>
- Sherry, M., Sheridan, J., & Jacono, D. L. (2013b). Characterisation of a horizontal axis wind turbine's tip and root vortices. *Experiment in Fluids*, 54, 1417. <http://dx.doi.org/10.1007/s00348-012-1417-y>
- Sicot, C., Devinant, P., Loyer, S., & Hureau, J. (2008). A study on stall-delay Investigation of the stall mechanisms. *Journal of Wind Engineering and Industrial Aerodynamics*, 96, 1320-1331, <http://dx.doi.org/10.1016/j.jweia.2008.01.013>
- Singh, R. K., & Ahmed, M. R. (2013). Blade design and performance testing of a small wind turbine rotor for low wind speed applications. *Renewable Energy*, 50, 812-819, <http://dx.doi.org/10.1016/j.renene.2012.08.021>
- Suzan, A. T. (2014). Radical Innovations in Wind Turbine Blade Design, Master thesis, Tufts University.
- Velázquez, M. T., DelCarmen, M. V., Franikitancis, J. A., Pacheco, L. A. M., & Eslava, G. T. (2014). Design and Experimentation of a 1 MW Horizontal Axis Wind Turbine. *Journal of Power and Energy Engineering*, 2, 9-16, <http://dx.doi.org/10.4236/jpee.2014.21002>
- Wua, Y., Lee, H. M., & Tang, H. (2015). A study of the energetic turbulence structures during stall delay. *International Journal of Heat and Fluid Flow*, 54, 183–195. <http://dx.doi.org/10.1016/j.ijheatfluidflow.2015.05.013>
- Yu, G., Shen, X., Zhu, X., & Du, Z. (2011). An insight into the separate flow and stall delay for HAWT. *Renewable Energy*, 36, 69-76. <http://dx.doi.org/10.1016/j.renene.2010.05.021>

Copyrights

Copyright for this article is retained by the author(s), with first publication rights granted to the journal.

This is an open-access article distributed under the terms and conditions of the Creative Commons Attribution license (<http://creativecommons.org/licenses/by/3.0/>).